Max-Planck-Institut für Mathematik in den Naturwissenschaften Leipzig

Analysis of inverse stochastic resonance and long-term firing in Hodgkin-Huxley neurons

(revised version: April 2012)

by

Henry Tuckwell, and Jürgen Jost

Preprint no.: 13 2012

Analysis of inverse stochastic resonance and the long-term firing of Hodgkin-Huxley neurons with Gaussian white noise

Henry C. Tuckwell[1†], **Jürgen Jost** [2]

[1] Max Planck Institute for Mathematics in the Sciences
Inselstr. 22, 04103 Leipzig, Germany

[†] *Corresponding author*: tuckwell@mis.mpg.de

April 18, 2012

Abstract

In order to explain the occurrence of a minimum in firing rate which occurs for certain mean input levels μ as noise level σ increases (inverse stochastic resonance, ISR) in Hodgkin-Huxley (HH) systems, we analyse the underlying transitions from a stable equilibrium point to limit cycle and vice-versa. For a value of μ at which ISR is pronounced, properties of the corresponding stable equilibrium point are found. A linearized approximation around this point has oscillatory solutions from whose maxima spikes tend to occur. A one dimensional diffusion is also constructed for small noise. Properties of the basin of attraction of the limit cycle (spike) are investigated heuristically. Long term trials of duration 500000 ms are carried out for values of σ from 0 to 2.0. The graph of mean spike count versus σ is divided into 4 regions $R_1, ..., R_4$, where R_3 contains the minimum associated with ISR. In R_1 transitions to the basin of attraction of the rest point are not observed until a small critical value of $\sigma = \sigma_{c_1}$ is reached, at the beginning of R_2. The sudden decline in firing rate when σ is just greater than σ_{c_1} implies that there is only a small range of noise levels $0 < \sigma < \sigma_{c_1}$ where repetitive spiking is safe from annihilation by noise. The firing rate remains small throughout R_3. At a larger critical value $\sigma = \sigma_{c_2}$ which signals the beginning of R_4, the probability of transitions from the basin of attraction of the equilibrium point to that of the limit cycle apparently becomes greater than zero and the spike rate thereafter increases with increasing σ. The quantitative scheme underlying the ISR curve is outlined in terms of the properties of exit time random variables. In the final subsection, several statistical properties of the main random variables associated with long term spiking activity are given, including distributions of exit times from the two relevant basins of attraction and the interspike interval.

Keywords: Hodgkin-Huxley equations, inverse stochastic resonance, white noise

1 Introduction

The Hodgkin-Huxley [1] systems of ordinary and partial differential equations, based on the electrophysiology of the squid giant axon, are the cornerstone of mathematical models of single neurons as well as several types of cardiac cells. Recent such studies include those of Komendantov et al. [2] for hypothathalamic magnocellular neuroendocrine cells, Saarinen et al. [3] for cerebellar granule cells, Williams et al. [4] for ventricular myocytes, Kameneva et al. [5] for retinal ganglion cells and Drion et al. [6] for dopaminergic neurons. Many of these computational cell models contain 10 or more components as the important roles of many different ion channels have been discovered since the appearance of the HH model. Analysis of such higher-dimensional models is very complex as there may be 50 or more parameters in distinction to the relatively few in the 4-component Hodgkin-Huxley system. Since the latter does in fact embrace some of the basic firing properties of neurons in general, there has naturally been a large number of analyses and computational studies of the HH systems. These include both deterministic (for example, [7, 8, 9, 10, 11, 12]) and stochastic (for

example, [13, 14, 15, 16, 17]) modeling. There have also been experiments on the application of white noise to squid axon involving both subthreshold [18] and suprathreshold [19, 20, 21] responses. In the last of these references noise was shown be capable of silencing repetitive spiking, an extended study of this phenomenon being the subject of the present investigation.

In recent articles [23, 24, 25] we have explored the effects of both additive Gaussian white noise and conductance noise on repetitive firing in the Hodgkin-Huxley system. In the additive noise case for the ordinary differential equation (ODE) model, when the mean input current density μ is not far above the threshold of 6.4 μA/cm^2 for repetitive firing, the number of spikes in the first 500 or 1000 ms was found to undergo a pronounced minimum (ISR) as the noise level σ increased from zero [23]. The minimum occurred around $\sigma = 0.35$. Guo [28] has recently found similar results for the HH ODE system with colored (Ornstein-Uhlenbeck process) noise. Similar results were found for the partial differential equation (PDE) system [24, 25] where the spatial distribution of the noise was also an important factor, which led to the distinction between the effects of noise on the instigation and propagation of spikes. Finally, as background material we refer the reader to some reviews [26, 27] of stochastic resonance, whose character is in a general sense the opposite to ISR.

1.1 Model description

In this article we restrict attention to the HH ODE system which corresponds to a uniformly polarized or "space-clamped" neuron. We use the original parameterization [1]. The system of stochastic differential equations was given in our previous articles but is repeated here for completeness and notation. With $V(t)$ the depolarization, in mV, and time t in ms

$$dV = \frac{1}{C}[\mu + \overline{g}_K n^4(V_K - V) + \overline{g}_{Na} m^3 h(V_{Na} - V) + g_L(V_L - V)]dt + \sigma dW \quad (1)$$

and for the auxiliary variables

$$dn = [\alpha_n(1-n) - \beta_n n]dt \quad (2)$$

$$dm = [\alpha_m(1-m) - \beta_m m]dt \quad (3)$$

$$dh = [\alpha_h(1-h) - \beta_h h]dt \quad (4)$$

where C is the membrane capacitance per unit area, μ, which may depend on t, is the mean input current density, $\overline{g}_K$, $\overline{g}_{Na}$ and g_L are the maximal (constant) potassium, sodium and leak conductances per unit area with corresponding equilibrium potentials V_K, V_{Na}, and V_l, respectively. The noise enters as the derivative of a standard Wiener process W and has amplitude σ. The auxiliary variables are $n(t)$, the potassium activation, $m(t)$, the sodium activation and $h(t)$, the sodium inactivation. The coefficients in the differential equations for the auxiliary variables as functions of depolarization are

$$\alpha_n(V) = \frac{10 - V}{100[e^{(10-V)/10} - 1]} \quad (5)$$

$$\beta_n(V) = \frac{1}{8}e^{-V/80} \tag{6}$$

$$\alpha_m(V) = \frac{25 - V}{10[e^{(25-V)/10} - 1]} \tag{7}$$

$$\beta_m(V) = 4e^{-V/18} \tag{8}$$

$$\alpha_h(V) = \frac{7}{100}e^{-V/20} \tag{9}$$

$$\beta_h(V) = \frac{1}{e^{(30-V)/10} + 1}. \tag{10}$$

The following standard parameter set was employed: $C = 1$, $g_K = 36$, $g_{Na} = 120$, $g_L = 0.3$, $V_K = 12$, $V_{Na} = 115$, and $V_L = 10$. The initial values are $V(0) = 0$ (rest) and for m, n and h the equilibrium values at rest, $m(0) = \alpha_m(0)/(\alpha_m(0)+\beta_m(0))$ etc. The units for these various quantities are as follows: all times are in msec, all voltages are in mV, all conductances per unit area are in mS/cm^2, C is in μF/cm^2, μ is in μA/cm^2 and σ is in μA msec$^{1/2}$ /cm^2.

2 Stable equilibrium point and limit cycle

When μ is above the critical value μ_{c_1} for repetitive firing (saddle-node bifurcation) and smaller than the value μ_{c_2} at which there is a subcritical Hopf bifurcation, there are two attractors consisting of a limit-cycle (action potential trajectory) and a stable equilibrium point.

2.1 Stable equilibrium point $\boldsymbol{x}^*$

Let us denote the random vector (V, n, m, h) by $\boldsymbol{X} = (X_1, X_2, X_3, X_4)$ and rewrite the system of equations as

$$dX_1 = F_1(\boldsymbol{X})dt + \sigma dW \tag{11}$$

$$dX_k = F_k(\boldsymbol{X})dt \tag{12}$$

where $k = 2, 3, 4$. Because a mean input current density of μ =6.8 μA/cm^2 was found to exhibit a pronounced minimum in firing as σ increased, we will focus on this value of μ unless stated otherwise.

Setting, with zero noise,

$$\boldsymbol{F}(\boldsymbol{x}^*) = \boldsymbol{0} \tag{13}$$

yields equilibrium points for the deterministic Hodgkin-Huxley system.

The Jacobian matrix at the equilibrium point is defined as

$$J(\boldsymbol{x}^*) = \left\{ \frac{\partial F_i}{\partial x_j} \right\}_{\boldsymbol{x}^*}, i, j = 1, ..., 4. \tag{14}$$

Its eigenvalues are denoted by $\lambda_k, k = 1, ..., 4$.

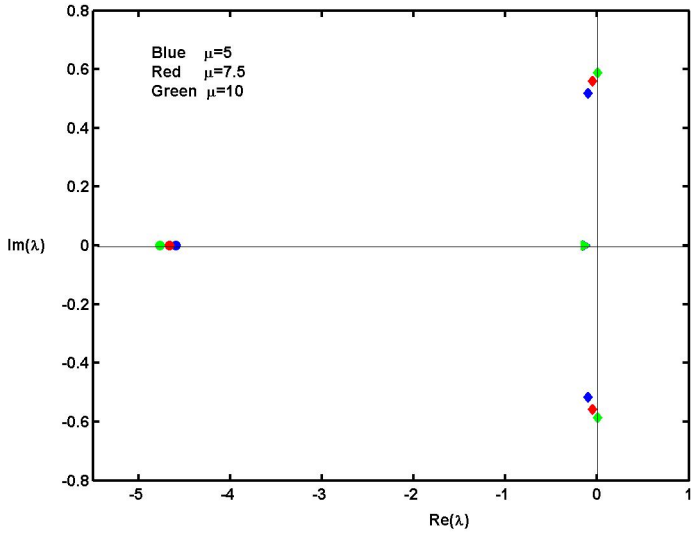

Figure 1: Eigenvalues in the complex λ-plane for three values of μ. The values of the real eigenvalue near $\lambda = -0.13$ are indistinguishable in this diagram.

Figure 1 shows the eigenvalues in the complex λ-plane for values of $\mu = 5$, below the critical value μ_{c_1}, $\mu = 7.5$, between the critical values μ_{c_1}, and μ_{c_2}, and $\mu = 10$ which is above μ_{c_2}. The nature of the critical point at the various values of μ can be readily seen. For the chosen value of $\mu = 6.8$, numerical evaluation gives an equilibrium point at

$$\boldsymbol{x}^* = (4.0536, 0.38107, 0.084327, 0.45129) \tag{15}$$

at which the components of F are

$$(-0.00000003084, 0.000024246, -0.0000013509, 0.0000048941) \tag{16}$$

Numerical evaluation of the eigenvalues of $J(\boldsymbol{x}^*)$ gives $\lambda_1 = -4.641$, the complex conjugate pair $\lambda_{2,3} = -0.630 \pm 0.548i$ and $\lambda_4 = -0.1323$. Hence $\boldsymbol{x}^*$ is an asymptotically stable spiral point.

2.2 The linear approximation

The system of stochastic ordinary differential equations for the process $\hat{\boldsymbol{X}}$ obtained by linearizing about $\boldsymbol{x}^*$ is

$$d\hat{X}_1 = \sum_{k=1}^{4} \frac{\partial F_1}{\partial x_k} \hat{X}_k dt + \sigma dW \tag{17}$$

$$d\hat{X}_j = \sum_{k=1}^{4} \frac{\partial F_j}{\partial x_k} \hat{X}_k dt, j = 2, 3, 4, \tag{18}$$

where the partial derivatives are evaluated at $\boldsymbol{x}^*$. The Jacobian is found numerically to be

$$10^2 * \begin{bmatrix} -0.010891 & -1.2764 & 1.2710 & 0.079467 \\ 0.000030551 & -0.0019202 & 0 & 0 \\ 0.00032794 & 0 & -0.034876 & 0 \\ -0.000044773 & 0 & 0 & -0.0012664 \end{bmatrix} \tag{19}$$

Note that the system (17)-(18) is linear and so $\hat{\boldsymbol{X}}$ is a Gaussian process. Using the theory in Rodriguez and Tuckwell [29], in the absence of an imposed spiking threshold, the exact distribution of $\hat{\boldsymbol{X}}$ can be found at any t. In the simulations in the sequel, the Euler scheme is used (see for example [30]).

Between spikes the linearized system (17)-(18) is expected to provide a reasonable approximation to the fully nonlinear system (1)-(4). This is clearly demonstrated by the two sets of sample paths shown in Figure 2. With input parameters $\mu = 6.8$, $\sigma = 0.6$, a time segment of length about 60 ms gave the sample path for V (that is, X_1) shown in the top part of the Figure. With the same path for the Wiener process (or the white noise), the sample path for the voltage $\hat{X}_1$ in the linearized system, with the same initial values, is seen in the lower part of Figure 2, to mimic closely that in the upper part. However, there is one very striking difference betwen the two paths as at about $t = 59$ ms the voltage in the linear system attains a local maximum and then decreases quite rapidly, continuing in an oscillatory fashion. In contrast, at about the same t and voltage values, a spike arises in the nonlinear system. However, these paths indicate that the time of spiking in the nonlinear system can be well approximated as the time at which the voltage in the linear system first attains a threshold value. Such a first passage time can be determined from the usual first exit time theory for diffusion processes.

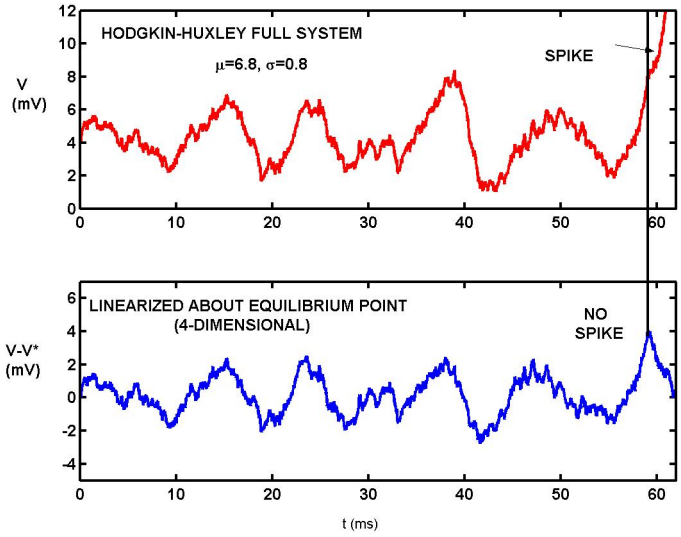

Figure 2: In the top part, voltage is plotted versus time for a sample path in the full nonlinear Hodgkin-Huxley system with the parameters shown. A spike forms near the end of the record. In the lower record is shown the voltage path for the system linearized about the stable equilibrium point. The Wiener path is the same in both records to enable a comparison to be made.

2.3 Numerical examples

Without an imposed threshold condition, no spikes are possible in the linearized stochastic system described by (17) and (18) because there is only a stable equilibrium point about which trajectories fluctuate. This is of course in distinction to the Hodgkin-Huxley system (with suitable input parameters) where trajectories may, if the fluctuations are large enough, give rise to spikes around the limit cycle. It is of interest to examine some statistical properties of the original process $\boldsymbol{X}$ in nonspiking periods. An example of paths with $\mu = 6.8$ and $\sigma = 0.1$ over a 50 ms nonspiking period is shown in Figure 3. The basic statistical properties of the components over a 500 ms time period are given in Table 1. In Table 2 are given the corresponding correlation coefficients.

Table 1: Statistics of variables during non-spiking period. $\mu = 6.8$, $\sigma = 0.1$

	Mean	Max	Min	St Dev	Coef Var
V	4.049	4.446	3.658	0.1337	0.0330
n	0.3811	0.3828	0.3795	6.61e-4	0.0017
m	0.0843	0.0874	0.0811	0.0012	0.0143
h	0.4515	0.4542	0.4488	0.001	0.0023

Table 2: Correlation coefficients during non-spiking period. $\mu = 6.8$, $\sigma = 0.1$

	V	n	m	h
V	1.0000	0.3068	0.9562	-0.2137
n	0.3068	1.0000	0.4649	-0.9894
m	0.9562	0.4649	1.0000	-0.3699
h	-0.2137	-0.9894	-0.3699	1.0000

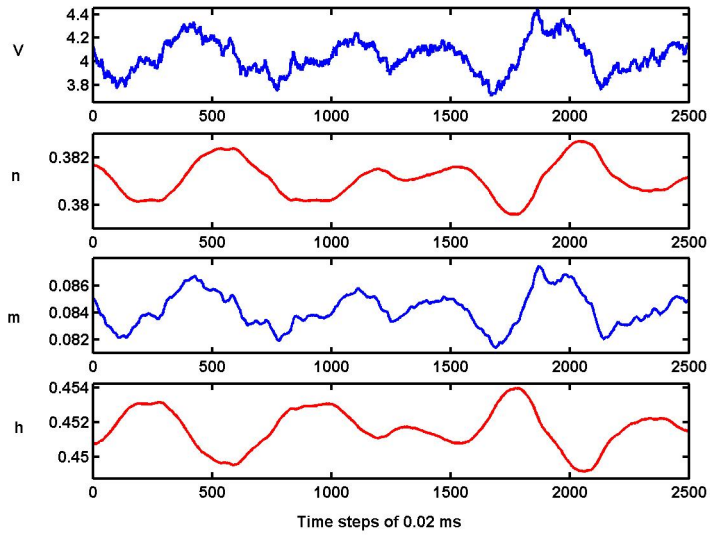

Figure 3: Sample paths for the 4 components of $\boldsymbol{X}$ over a 50 ms period during which there were no spikes. Input parameters $\mu = 6.8$ and $\sigma = 0.1$.

Tables 3 and 4 give the statistical properties during a 500 ms nonspiking time period when the noise level is $\sigma = 0.6$.

Table 3: Statistics of variables during non-spiking period. $\mu = 6.8$, $\sigma = 0.6$

	Mean	Max	Min	St Dev	Coef Var
V	4.149	8.962	-0.206	1.301	0.314
n	0.383	0.419	0.368	0.0077	0.020
m	0.0859	0.1393	0.0538	0.0126	0.147
h	0.4471	0.4668	0.3883	0.0122	0.0274

Table 4: Correlation coefficients, $\mu = 6.8$, $\sigma = 0.6$

	V	n	m	h
V	1.0000	0.3505	0.9690	-0.2408
n	0.3505	1.0000	0.5284	-0.9854
m	0.9690	0.5284	1.0000	-0.4272
h	-0.2408	-0.9854	-0.4272	1.0000

There are two very noticeable features of the sample paths in the nonspiking periods examined. Firstly, the oscillatory character of the paths, which is traceable to the eigenvalues of the Jacobian at the equilibrium point. Secondly, the strong positive correlation between V and m and the strong negative correlation between n and h.

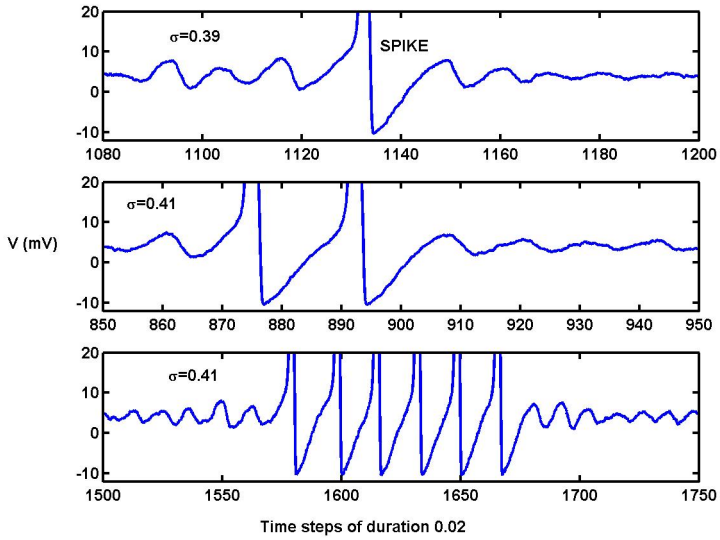

Figure 4: Showing how single, double and multiple spikes arise from oscillations in the nonlinear full Hodgkin-Huxley system with noise. $\mu = 6.8$

The oscillatory nature of the paths can never be captured in the standard integrate and fire models nor the leaky integrate and fire models [31]. When the noise is sufficiently large to make for fairly frequent spiking, the times of spiking must tend to arise at the maxima in the oscillations of V. This is seen dramatically in Figure 4 and in Figure 2 of the previous subsection.

2.4 A one-dimensional diffusion

Examination of the statistical properties of the process given in Tables 1 and 2 shows that for small noise the coefficients of variation of n and h are an order of magnitude smaller than those for V and m and that the correlation coefficient of V and m is close to unity. These observations make it reasonable to consider a 1-dimensional approximation $\hat{V}$ to the HH system in which a constant $\overline{n} \approx n$ and a constant $\overline{h} \approx h$, with $m = kV$, where k is another constant. These approximations lead, on putting $C = 1$ in (1), to the following stochastic differential equation for $\hat{V}$,

$$d\hat{V} = (\mu + c_1 - c_2\hat{V} + c_3\hat{V}^3 - c_4\hat{V}^4)dt + \sigma dW, \tag{20}$$

where

$$c_1 = \overline{g}_K\overline{n}^4V_K + g_LV_L \tag{21}$$

$$c_2 = \overline{g}_K\overline{n}^4 + g_L \tag{22}$$

$$c_3 = \overline{g}_{Na}k^3\overline{h}V_{Na} \tag{23}$$

$$c_4 = \overline{g}_{Na}k^3\overline{h}. \tag{24}$$

Standard theory gives for such a diffusion that the mean exit time from a value $x \in (a, b)$ to outside this interval satisfies the ordinary differential equation

$$(\sigma^2/2)M'' + (\mu + c_1 - c_x + c_3x^3 - c_x^4)M' = -1, x \in (a, b), \tag{25}$$

where primes denote differentiation, along with suitable boundary conditions. Note that it is impossible for the solutions of any one-dimensional temporally homogeneous system to oscillate. Preliminary investigations of the validity of this approximation were made using values for $\mu = 6.8$ and $\sigma = 0.1$ (see Tables 1 and 2) but a detailed study will be reported in a subsequent article.

2.5 The limit cycle and its basin of attraction

With constant input current density in the interval $[\mu_{c_1}, \mu_{c_2})$, repetitive spiking may occur with a fixed period. For $\mu = 6.8$ and no noise the period is about 17.65 ms. The limit cycle is in 4-space but we here show in the upper part of Figure 5 the projection of the limit cycle obtained by plotting n versus V. In the lower part of the figure is shown the position of the stable equilibrium point, $\boldsymbol{x}^*$, here designated R, for the same value of μ. It can be seen that the limit cycle approaches quite close to R. In a previous article in which the moment method was used to explore the effects of noise on HH spiking [23]Kate Smith-Miles, we

heuristically estimated the basin of attraction of the stable equilibrium point. Part of the basin of attraction of the limit cycle can be numerically estimated by taking the union of all stochastic paths which do not collapse to the stable equilibrium point. As explained later, there are ranges of values of σ where the stochastic paths have this property and Figure 6 shows a sample of such paths for various such σ. Here paths were taken over 1000 msec involving about 50 spikes for values of σ ranging from 0.05 to 0.25. This picture gives an idea of how far off the deterministic limit cycle a path may wander without entering the basin of attraction of the stable equilibrium point. The variability of paths is relatively small.

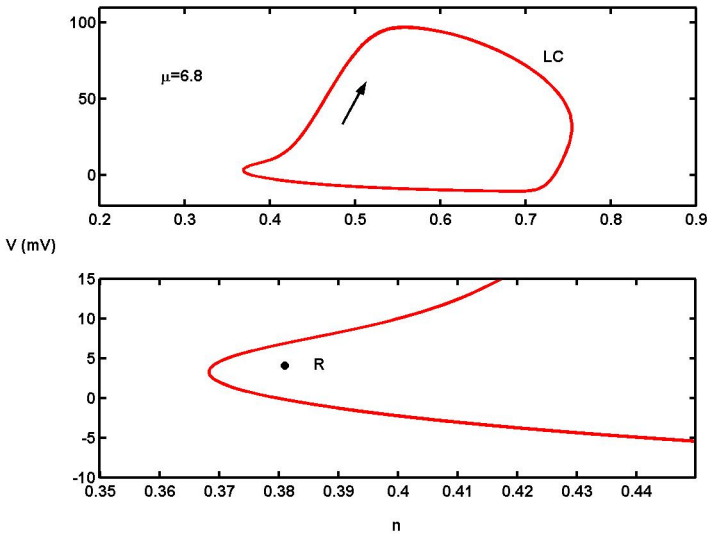

Figure 5: In the top part, voltage is plotted versus potassium activation variable for the deterministic path of repetitive spikes, depicting the limit cycle for the HH ODE system with $\mu = 6.8 > \mu_{c_1}$. In the lower part the limit cycle is magnified in the vicinity of the stable rest point.

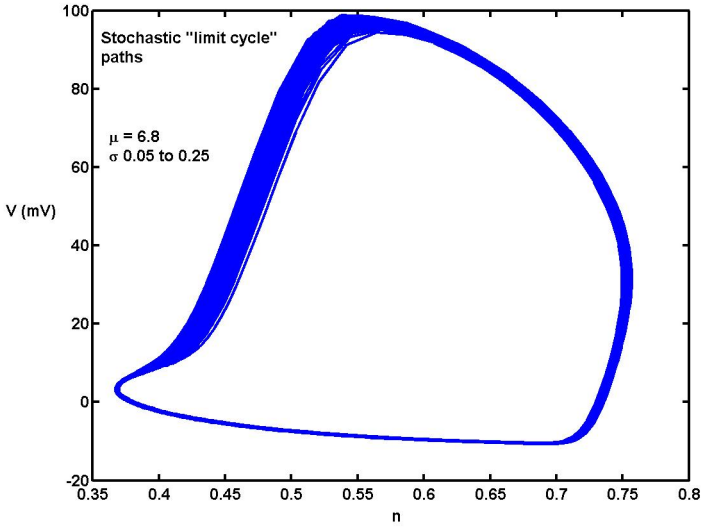

Figure 6: The union of many stochastic paths for values of the noise parameter σ for which paths did not collapse into the stable point in a time interval of at least 1000 ms.

Another way to see the limited variability of the times to complete a spike orbit (limit cycle) is displayed in Figure 7. Here spikes were observed during repetitive firing during periods in which no transitions to the basin of attraction of the rest point occurred, with noise levels from $\sigma = 0$ to $\sigma = 0.4$. The statistical properties of the interspike interval (ISI) are shown in the Figure. The most salient feature is that the mean ISI is practically constant (blue triangles) as the noise varies, staying in the interval $[17.58, 17.82]$ for these values of σ. Naturally the standard deviation of the ISI increases (green squares) as σ increases, the maximum ISI increases /red circles) and the minimum ISI decreases (black diamonds).

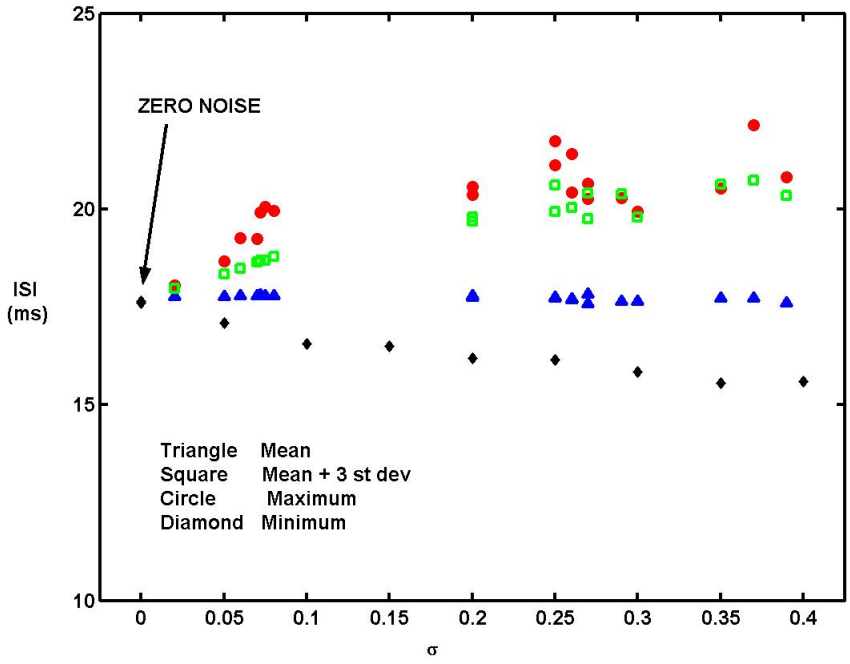

Figure 7: Some statistical measures of the ISI during repetitive spiking at various noise levels with $\mu = 6.8$. For $\sigma = 0$, there is no variability. The mean ISI is shown with (blue) triangles, the (green) squares denote the mean + 3 standard deviations, the (red) circles denote the maxima and the (black) diamonds denote the minima. Until σ is about 0.07, there are no cessations of spiking up to 500000 ms.

Examples of distributions of the ISI during repetitive spiking at small noise levels are shown in Figure 8. In the top panel is an ISI histogram for a noise level ($\sigma = 0.07$) at which there is apparently no cessation of spiking over extremely long (infinite?) time periods with 28429 ISIs in 500000 ms. The distribution is roughly Gaussian and has a mean of 17.59 ms and a standard deviation of 0.221 ms. For the second histogram shown, $\sigma = 0.085$, which is just greater than the critical value at which spiking may stop in a finite time. The number of spikes is only 4397 and the mean and standard deviation of the ISI are 17.60 ms and 0.276 ms, respectively. The distribution of the ISI is practically the same in both cases.

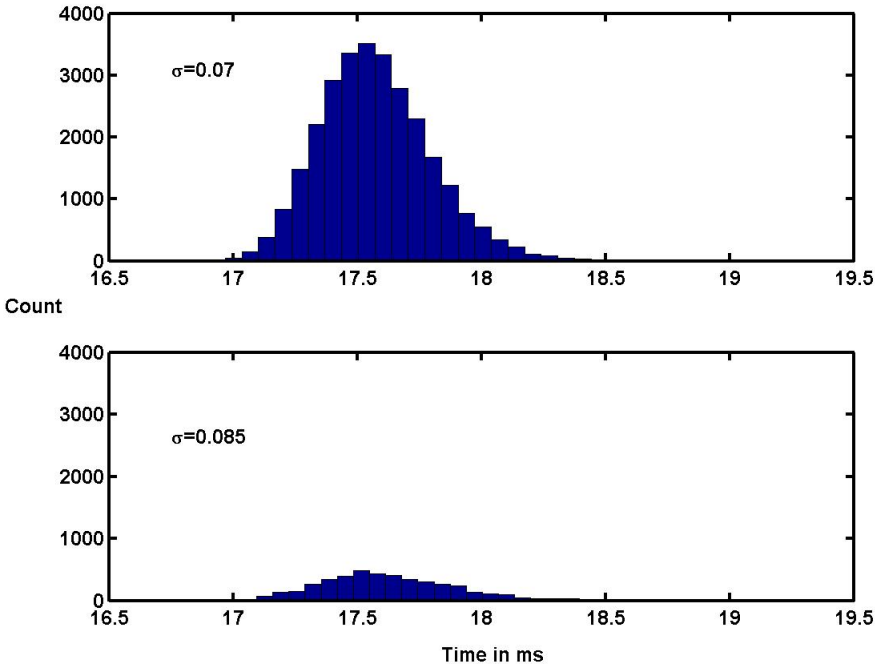

Figure 8: Examples of histograms of the ISI during repetitive spiking at two small noise levels. Top, $\sigma = 0.070$; bottom, $\sigma = 0.085$. For $\sigma = 0.07$ there are no cessations of spiking up to 500000 ms whereas for $\sigma = 0.085$ firing stops after about 4400 spikes.

3 Results on spiking for the HH system and inverse stochastic resonance

In the following it is assumed that μ is such that repetitive spiking does in fact occur. In relation to the stochastic paths for the HH system of stochastic equations we define the following two random variables.

Firstly, the exit time of the process to escape from the basin of attraction B_L of the limit cycle L to that B_R of the rest point R is by

$$T_{L\to R}(\boldsymbol{x}_0), \boldsymbol{x}_0 \in B_L \tag{26}$$

where $\boldsymbol{x}_0 = (V_0, n_0, m_0, h_0)$ is an initial point. Secondly the exit time for the process to escape from the basin of attraction B_R of R to that of the limit cycle is

$$T_{R\to L}(\boldsymbol{x}_0), \boldsymbol{x}_0 \in B_R. \tag{27}$$

Using the standard theory for diffusion processes, Kolmogorov second order partial differential equations for the moments and distributions of these quantities as a function of initial values were described in our previous work [22]. However, any attempt to solve these equations analytically or even by numerical methods for PDEs, apart from being a formidable task, requires an exact or even approximate knowledge of the two basins of attraction which is unfortunately not presently available. In fact the probabilistic nature of B_L and B_R is not completely understood because it seems that for small enough noise, at least for some values of μ, escape from B_L may be impossible, not being observed in extremely long time periods and similarly, for particular ranges of σ, for escape from B_R.

3.1 Long term trials and data collected

We are interested in obtaining samples of meaningful sizes for the above random variables and determining their properties, mainly as a function of σ. Since some of the exits from one basin of attraction to the other are, for some values of σ, very rare events the simulations of solutions of the full stochastic HH system have to be performed over very long time periods. These were chosen to be 500000 ms or about 8 minutes and 20 seconds with a timestep of 0.065 ms. Results for the 500000 ms interval were obtained as the union of 100 trials of length 5000 ms, where the final values of V, n, m, h from any trial were used as the initial values for the next trial. Then the data on t, V, n, m, h for the 100 trials were concatenated to give 5 single vectors each with over 7.5 million elements. The records for V versus t were analyzed to determine the times of occurrence of spikes and from these the exit times and interspike intervals were determined. In total, 50 trials of length 500000 were simulated.

3.2 All spikes

The numbers of spikes were recorded in each of 50 trials of length 500000 ms for 40 values of σ. The mean number of spikes, denoted by E[NSP], is plotted against σ in Figure 9. In the top panel all results are included, whereas in the lower left panel detail is shown for $0 \leq \sigma \leq 0.1$ and in the lower right panel, for $0.1 \leq \sigma \leq 0.5$.

The general form of the plot of E[NSP] versus σ is similar to that in Figure 5 of [22] where the total time period was much less at 1000 ms. Thus, Figure 9 exhibits the phenomenon of inverse stochastic resonance, which refers to a firing rate which, as noise level increases, at first declines to a minimum and then becomes greater. However, Figure 9 shows more detail and reveals 4 distinct regimes marked R_1,...,R_4. In region R_1, which extends from the deterministic setting of $\sigma = 0$ to very close to $\sigma = 0.07$, the noise is almost without effect and the number of spikes is always close to that for the zero noise, 28431. Region R_2 is characterized by a rapidly falling number of spikes as σ increases from 0.07 to 0.14. At the latter value of σ the mean number of spikes is 104.8 which is about 0.4% of the maximum value. In region R_3, from $\sigma = 0.15$ to $\sigma = 0.35$,

E[NSP] stays below 100 with a broad minimum of about 9.5 spikes (0.03% of the maximum) around $\sigma = 0.295$ to 0.300. By $\sigma = 0.375$, the beginning of region R_4, the mean number of spikes has reached over 120 and then increases sharply and eventually at a slower rate to reach 25883 around $\sigma = 2$.

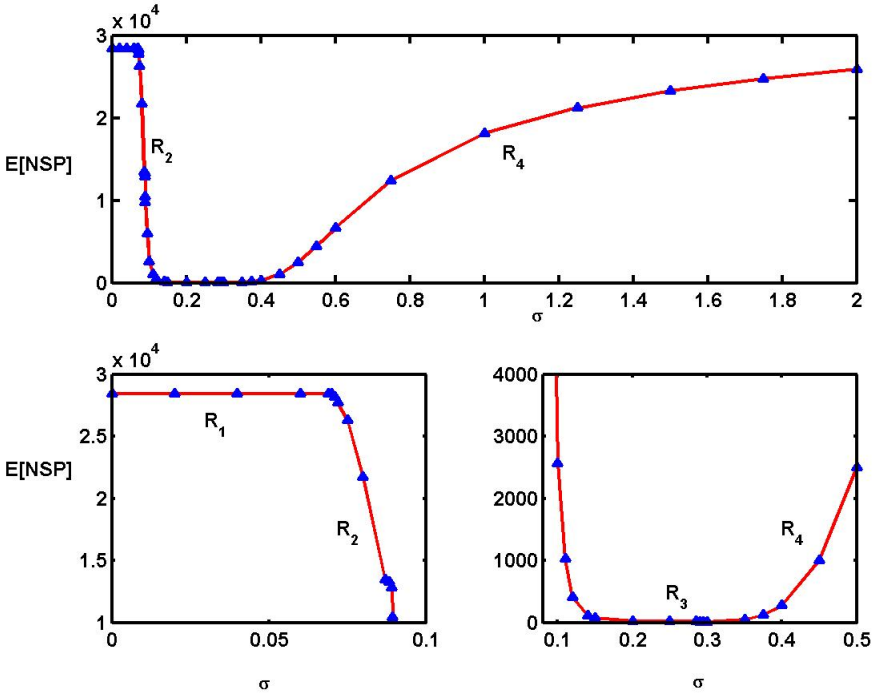

Figure 9: The dependence on the noise parameter σ of the mean of the total number of spikes E[NSP] in a time interval of length 500000 ms in the nonlinear HH system. Here $\mu = 6.8$ with 50 trials at each point. The values of σ are divided into 4 regimes designated R_1 to R_4. In the top panel, results are given for all values of σ. In the lower left panel the detail of R_1 and the start of R_2 are shown. In the lower right panel, the detail of R_3 and the start of R_4 are shown.

3.3 Underlying scheme for ISR

The following observations constitute a basis for ISR which occurs at some values of μ in the HH system described by Equations (1)-(4). We define two critical values σ_{c_1} and σ_{c_2} of the noise parameter σ, with $0 < \sigma_{c_1} < \sigma_{c_2} < \infty$. σ_{c_1} and σ_{c_2} depend on μ, and are only relevant above the critical value for repetitive firing and possibly for selected initial values of the process (see [22]). With reference to the two random variables defined by (26) and (27), but without any specific

values of $\boldsymbol{x}_0$, we have the following, as schematized diagrammatically in Figure 10.

$\mathbf{0 < \boldsymbol{\sigma} < \boldsymbol{\sigma}_{c_1}}$.
Repetitive spiking continues, presumably indefinitely.
The probability of a transition from B_L to B_R at any time is apparently zero.
The expectation of $T_{L\to R}(\boldsymbol{x}_0), \boldsymbol{x}_0 \in B_L$, is effectively infinite.

$\boldsymbol{\sigma}_{c_1} < \boldsymbol{\sigma} < \boldsymbol{\sigma}_{c_2}$.
Repetitive spiking ceases at some random time $T_1 < \infty$.
The probability of a transition from B_L to B_R is greater than zero and increases with noise level.
The expectation of $T_{L\to R}(\boldsymbol{x}_0), \boldsymbol{x}_0 \in B_L$, is finite and and tends to decrease with increasing σ (see Figure 12).
After a transition from B_L to B_R, the probability of the reverse transition from B_R to B_L is effectively zero.
The expectation of $T_{R\to L}(\boldsymbol{x}_0), \boldsymbol{x}_0 \in B_R$, is apparently infinite.
After the cessation of repetitive spiking, there is no more spiking, at least in any observed time period.

$\boldsymbol{\sigma} > \boldsymbol{\sigma}_{c_2}$.
After a transition from B_L to B_R, the probability of a transition from B_R to B_L is greater than zero and tends to increase as σ incresases.
The expectation of $T_{R\to L}(\boldsymbol{x}_0), \boldsymbol{x}_0 \in B_R$, is finite and tends to decrease as σ increases (see Figure 13).
After a transition back from B_R to B_L, the reverse transition occurs with non-zero pobability, followed again by a transition from B_L to B_R and so forth, indefinitely.
Epochs of spiking and nonspiking alternate with variable durations which tend to become shorter as σ increases.

Figure 10 illustrates some of these aspects. The bottom panel shows part of the actual E[NSP] curve (normalized) from Figure 9 and the approximate values of σ_{c_1} and σ_{c_2} are obtained from this curve. In the top panel, the probabilities of transitions from B_L to B_R and B_R to B_L are indicated as commencing to increase from zero at the two critical values of σ and rising to unity, although this final value depends on the initial value $\boldsymbol{x}_0$ which is not fixed throughout. In the middle panel, descriptions of the expectations of the exit times from B_L and B_R are given.

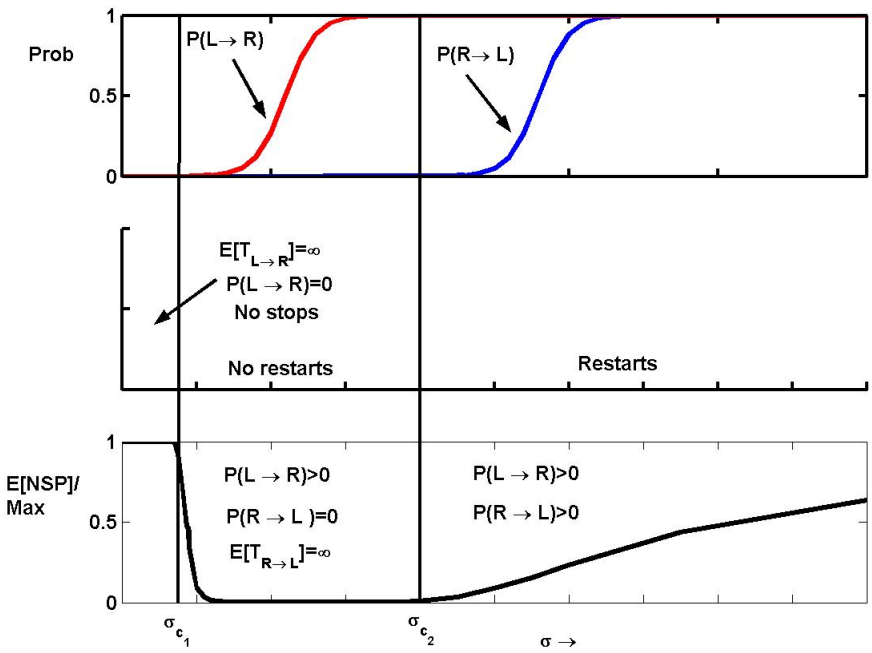

Figure 10: A schematic representation for the transitions underlying ISR. There are shown two critical values of the noise parameter σ and the probabilities of transitions between the basins of attraction B_L and B_R of the limit cycle and rest point are sketched in the top panel for the various ranges of values of σ. In the bottom panel is shown the normalized expected number of spikes obtained by simulation over 500000 ms for $\mu = 6.8$, a value of μ at which ISR had been found to be pronounced.

The scheme given in Figure 10 is in accordance with the results for sample paths of V for simulated spike trains shown in Figure 11. Here the time periods are all 500000 ms but in the top two records time is only shown to 2000 ms. The very small noise case gives apparently indefinite repetitive spiking. Somewhat larger noise leads to an initial isolated burst followed by silence, possibly for an infinite time. Increasing the noise further leads to occasional bursting and eventually the frequent bursting case occurs.

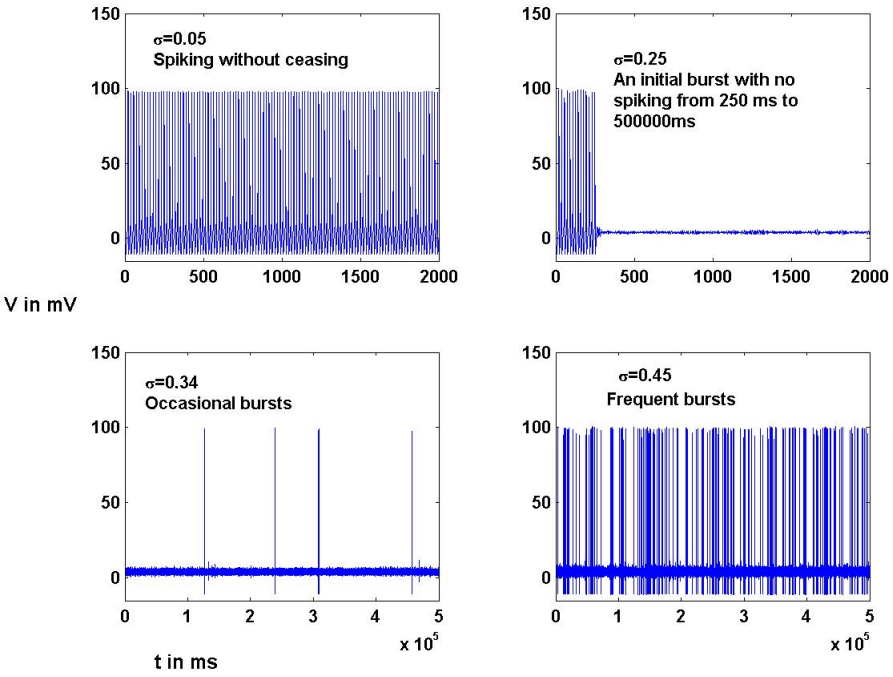

Figure 11: Illustrating the 4 basic patterns of spiking activity. Top left: $\sigma = 0.05$. Incessant spiking, at least to 500000 ms. Top right: $\sigma = 0.25$. One initial burst with no further spikes, at least to 500000 ms. Bottom left: $\sigma = 0.34$. Occasional bursts with separations of order 100000 ms. Bottom right: $\sigma = 0.45$. Frequent bursts.

3.4 Some statistics of $T_{L\to R}$ and $T_{R\to L}$

In this subsection results on certain statistical aspects of the underlying random variables $T_{L\to R}$ and $T_{R\to L}$, defined by (26) and (27), obtained from the long-term simulation of the HH system (1)-(4) are given.

3.4.1 Escape time from B_L

During repetitive spiking the trajectories of the process do not deviate much from the deterministic limit cycle as illustrated in Figure 6. It is assumed that there is a well-defined but unkown set in (V, n, m, h)-space, denoted by B_L, containing the deterministic repetitive spiking trajectory, which is called the basin of attraction of the limit cycle. This implies that if the process started in B_L, then, with no noise, the path would approach the limit cycle. With noise, trajectories may escape from B_L whereupon they enter the basin of attraction

B_R of the stable equilibrium point. The nature of B_L is unknown and it is not clear that it is a regular open set because if it was it is likely that escape from it would occur eventually with probability one no matter how small the noise level. Thus, even though it seems that for $\sigma < \sigma_{c_1}$, $P(L \to R) = 0$ and $\mathrm{E}[T_{L\to R} = \infty]$, it may be the case that $P(L \to R)$ is so small for small enough σ that the event of this escape is unlikely to be observed in the course of feasible simulations. It is a remaining mathematical challenge to ascertain the veracity of these remarks.

Notwithstanding these uncertainties, the mean value of $\mathrm{E}[T_{L\to R}]$ of the exit time from B_L was estimated from sample paths and the results are shown for $\sigma \geq 0.2$ in Figure 12. For these noise levels the mean exit time declines rapidly from very large values to a minimum of about 57 ms at $\sigma = 1.25$. Thereafter, $\mathrm{E}[T_{L\to R}]$ seems to increase slightly to about 72 ms at $\sigma = 2$.

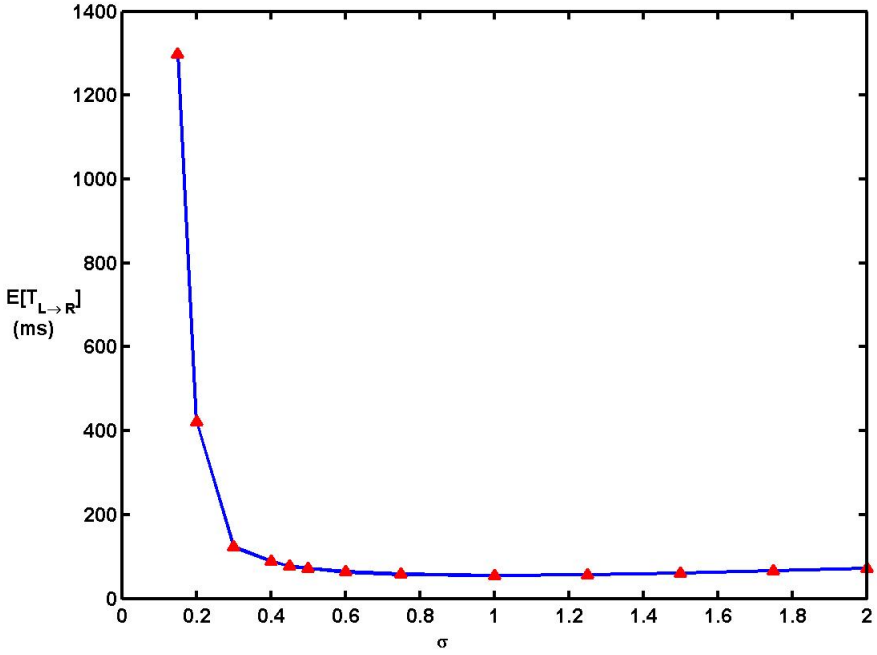

Figure 12: The dependence on the noise parameter σ of the expectation $\mathrm{E}[T_{L\to R}]$ of the random variable which is the time of exit of the process from the basin of attraction of the limit cycle to that of the stable rest point. 50 trials at each point with $\mu = 6.8$. For values of σ less than a critical value $\sigma_{c_1} \approx 0.07$ the value of this expectation is effectively infinite. Extremely large values which occurred for $\sigma_{c_1} < \sigma < 0.2$ are not shown.

3.4.2 Escape time from B_R

The basin of attraction of the stable rest point is also unknown exactly. Figures 13 and 14 show estimates of the mean and standard deviation of $T_{R\to L}$ over various ranges of values of σ. Again, it is not known with certainty, but it appears that the probability of escape from B_R to B_L is zero (or extremely close to zero) until $\sigma \geq \sigma_{c_2}$. In Figure 13, the mean is shown dropping from values of order 300000 ms at $\sigma = 0.25$ to eventually reach values about 30 ms at $\sigma = 2$. Figure 14 shows corresponding results for the standard deviation, but only for $\sigma \geq 0.35$ because sample sizes were too small for lesser values of the noise parameter. In the lower panel of Figure 14 is shown the dependence of the coefficient of variation of $T_{R\to L}$ on noise level. It can be seen that there is an initial increase in this quantity until a maximum is attained at about $\sigma = 0.5$, whereupon it declines monotonically.

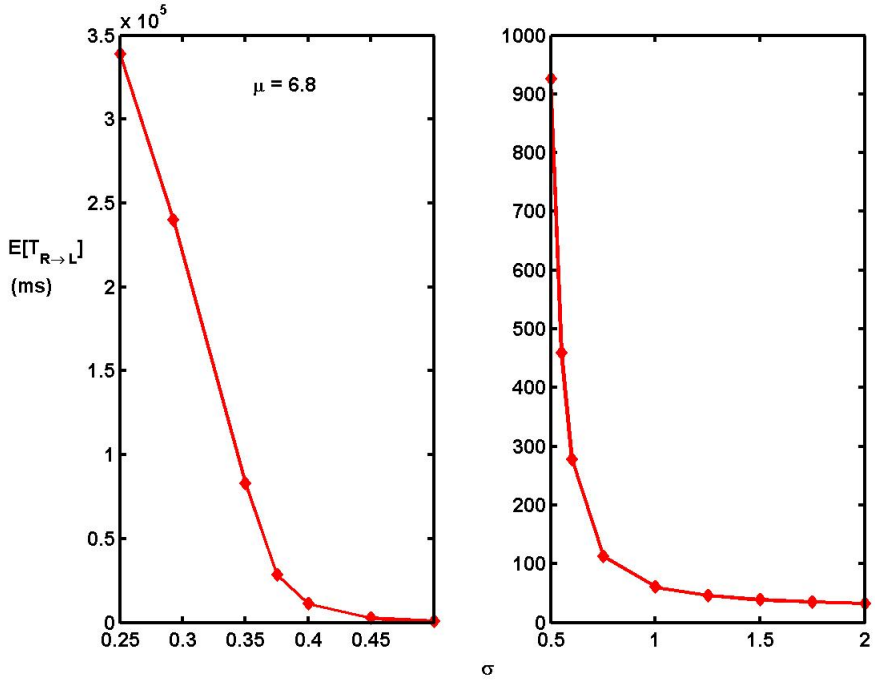

Figure 13: The dependence on the noise parameter σ of the expectation $\mathrm{E}[T_{R\to L}]$ of the random variable which is the time of exit of the process from the basin of attraction of the stable rest point to that of the limit cycle. Here $\mu = 6.8$. 50 trials at each point. For values of σ less than some value just less than 0.25 the value of this expectation is effectively infinite.

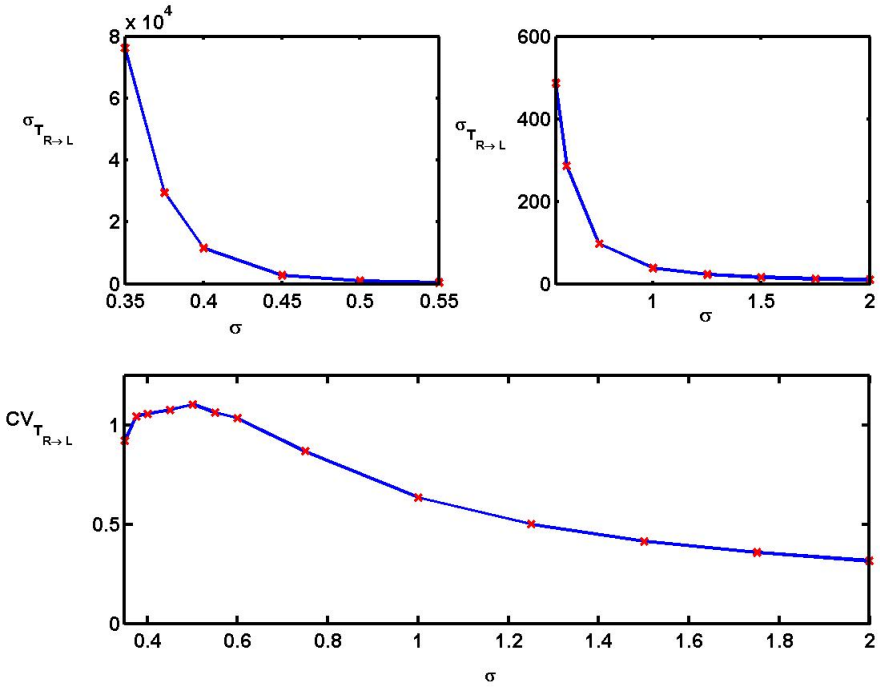

Figure 14: *Top two panels.* The dependence on the noise parameter σ of the standard deviation $\sigma_{T_{R\to L}}$, of the random variable which is the time of exit of the process from the basin of attraction of the stable rest point to that of the limit cycle. Here $\mu = 6.8$. 50 trials at each point. *Bottom panel.* The coefficient of variation of the random variable $T_{R\to L}$ as a function of σ.

3.4.3 Distributions

There are three main random variables of interest in relation to the empirical spike trains obtained in this study. These are the previously defined exit times $T_{L\to R}$ and $T_{R\to L}$ and in addition the general ISI for the whole train. Examples of histograms of these random variables are shown in Figure 15. In all cases the results for 50 trials of duration 500000 ms are combined. In Figure 15A is given a histogram for all ISIs for $\sigma = 0.2$. This occurs in region R_3 of Figure 9, where there are very few spikes, all with short ISIs as there are no returns to B_L fron B_R. The histogram is of the same nature as those in Figure 8. See also Figure 7.

In Figure 15C the raw histogram is shown for all ISIs with $\sigma = 0.350$. There is a preponderance of small intervals and then an exponential-type distribution of longer (> 21.5 ms) intervals as depicted in Figure 15E. The tail of the exponential distribution is very long and extends out to about 500000 ms which is

the limit in these simulations. The distribution depicted in Figure 15E is close to the actual distribution of $T_{R\to L}$ for this value of σ. Similar remarks apply to the pairs of Figures 15B and 15D ($\sigma = 0.375$) and 15F and 15G ($\sigma = 0.5$). In the final plot of Figure 15H, the number of spikes has become enormous and the majority of ISIs are less than 50 ms as expected for $\sigma = 1$ which is in region R_4 of Figure 9. In the histograms of Figure 15 C, B, F and H, there are small bin counts out to very large times and these are not visible compared to the large bin count at short intervals. However, they are visible at relatively small values in the truncated histograms.

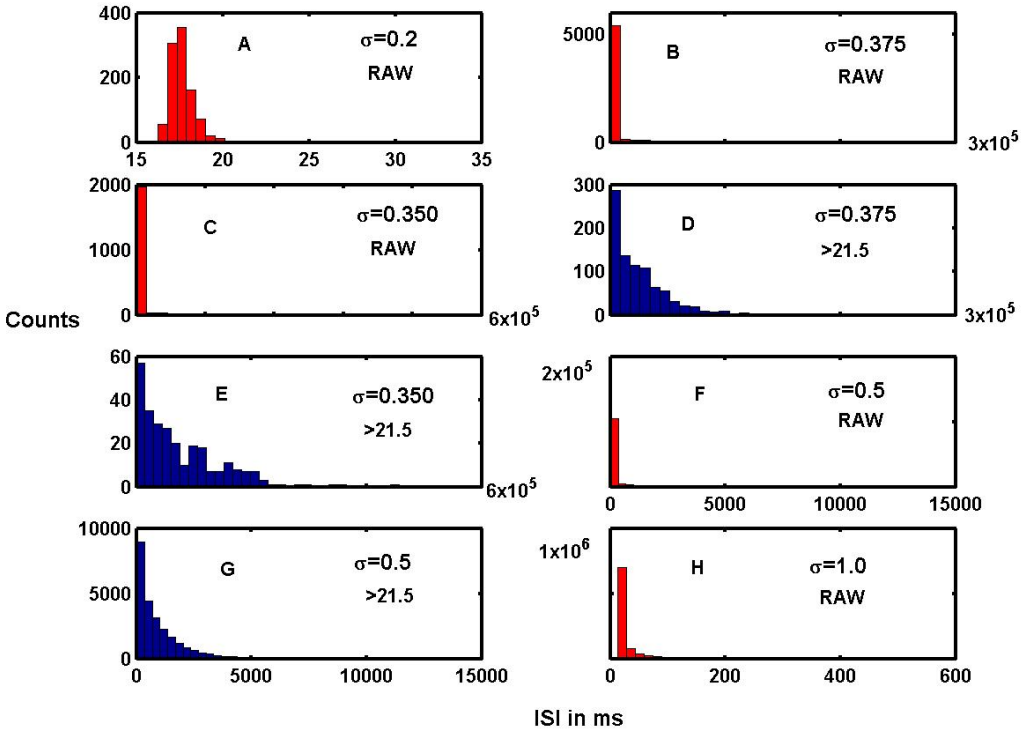

Figure 15: Examples of distributions (histograms) of ISIs and exit times from B_R based on 50 trials (data pooled) of length 500000 ms. Red histograms, raw data. Blue histograms, ISIs truncated at 21.5 ms. A. Raw data for $\sigma = 0.2$. B. Raw data for $\sigma = 0.375$. C. Raw data for $\sigma = 0.350$. D. Truncated data for $\sigma = 0.375$. E. Truncated data for $\sigma = 0.350$. F. Raw data for $\sigma = 0.5$. G. Truncated data for $\sigma = 0.5$. H. Raw data for $\sigma = 1.0$.

To complete the picture for the distributions of the three key random variables, Figure 16 shows histograms of mean numbers of spikes per burst for two values, 0.4 and 1.0, of σ. If these are multiplied by the mean ISI within bursts,

which is about 17.6 ms, the mean times spent in the basin of attraction of the limit cycle (B_L) and hence of $T_{L\to R}$ are estimated. For smaller σ some very large means were obtained (not shown). Noticeable in Figure 16 is the smaller magnitude and small variability when $\sigma = 1.0$ compared to $\sigma = 0.4$. The distributions in both cases shown are approximately Gaussian which may be compared with the exponential-types shown in Figures 15 D, E and G.

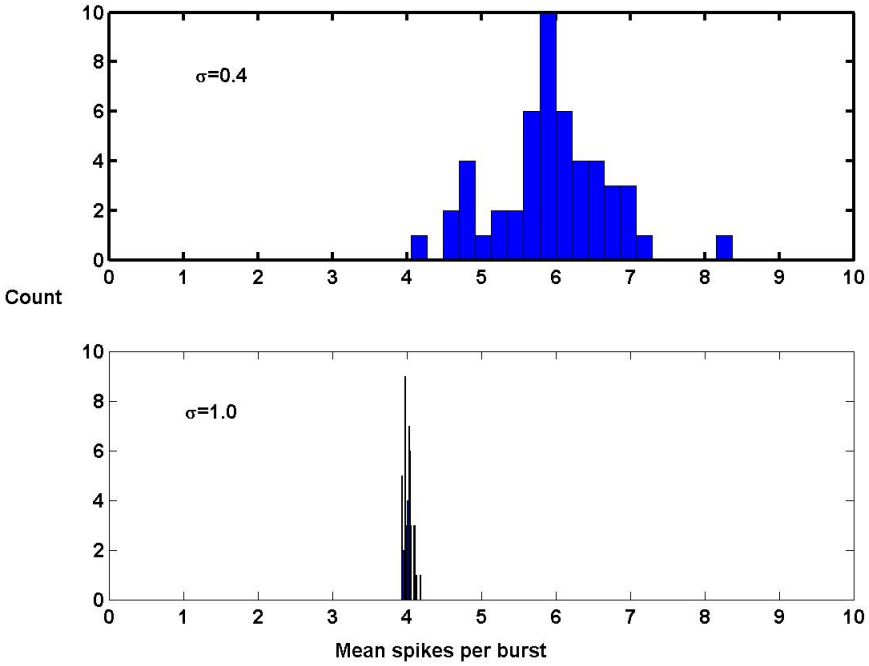

Figure 16: Histograms of mean numbers of spikes per burst, which indicate magnitudes of exit times from B_L to B_R. based on 50 trials of length 500000.

4 Discussion

The inhibitory effects of noise on repetitive spiking in squid axon, on whose electrophysiology the HH system is based, were well documented experimentally by Paydarfar et al. [21]. The first theoretical evidence of ISR in the full HH system was obtained for $\mu = 5$ in the non-repetitive spiking mode [32] (Figure 2), as it was found that there was a maximum in the mean ISI at small values of σ. Subsequently ISR has been demonstrated for repetitive spiking in both the HH system of ODEs and PDEs [22, 24, 25, 28]. In addition to using the standard initial conditions and additive noise, in [22] the phenomenon was confirmed with respect to random initial conditions and conductance-based input (synaptic

noise). Some theory of ISI was also outlined [22] in terms of bifurcations in the HH system [7, 10, 33] and of the exit times [34] from the basins of attraction of a stable equilibrium point and a limit cycle. However the simulations were over relatively short time periods and the statistical details of the exit times were not explored in detail.

In this article we have first explored the properties of the stable equilibrium point in depth. Linearizing the stochastic HH system about that point gave an approximate system of stochastic differential equations whose fluctuating oscillatory solutions were found to mimic those of the full system in nonspiking periods. The oscillations are evidently an integral part of firing in the HH system with the considered parameters, because spikes did tend to emerge at the maxima. The distribution of ISIs with trajectories not departing greatly from the limit cycle for very small noise was estimated and is, as perhaps expected, Gaussian-like.

Long-term simulations, to 500000 ms were performed with $\mu = 6.8$ for many values of the noise parameter σ. Four ranges of values of σ were distinguished, based on mean total numbers of spikes. These regions were denoted $R_1, ..., R_4$ in Figure 9. Two critical values of σ were also apparent, denoted by $0 < \sigma_{c_1} < \sigma_{c_2} < \infty$. A detailed discussion of the mechanisms underlying ISR in terms of these critical values was given in Section 3.3. It is not certain whether escape from the basin of attraction of the limit cycle can ever occur when $\sigma < \sigma_{c_1}$ or whether escape from the basin of attraction of the stable equilibrium point can ever occur when $\sigma_{c_1} < \sigma < \sigma_{c_2}$, but these events were never observed in 50 trials of length 500000 ms with several values of σ. The most dramatic finding in the present work is the sudden decline in firing rate when the noise is just greater than σ_{c_1}, which implies that there is only a small range of noise levels $0 < \sigma < \sigma_{c_1}$ where repetitive spiking is safe from annihilation by noise.

On a final note, we remark that there are other ways in which noise may occur in neuronal dynamical systems such as HH. One of these is as synaptic noise which we included in a previous article [22] and found results of the same nature as for additive noise. Another is ion channel noise which has been explored mathematically in the HH system [16] and its effects on spiking determined [35, 36]. For the latter type of noise, no investigations into the possibility of ISR have, as far as we know, been made, but considering the robustness of the phenomenon found under a variety of conditions so far it is likely that ISR would also occur in the case of channel noise.

References

[1] A.L. Hodgkin, A.F. Huxley, A quantitative description of membrane current and its application to conduction and excitation in nerve, J. Physiol. 117 (1952) 500-544.

[2] A.O. Komendantov, N.A.Trayanova, J.G. Tasker, Somato-dendritic mechanisms underlying the electrophysiological properties of hypotha-

lamic magnocellular neuroendocrine cells: A multicompartmental model study. J. Comput. Neurosci. 23 (2007) 143-168.

[3] A. Saarinen, M-L.Linne, O. Yli-Harja, Stochastic differential equation model for cerebellar granule cell excitability. PLoS Comp. Biol. 4 (2008) e1000004.

[4] G.S.B. Williams, G.D. Smith, E.A. Sobie, M.S. Jafri MS, Models of cardiac excitation-contraction coupling in ventricular myocytes. Math. Biosci. 226 (2010) 1-15.

[5] T. Kameneva, H. Meffin, A.N. Burkitt, Modelling intrinsic electrophysiological properties of ON and OFF retinal ganglion cells. J. Comp. Neurosci. 31 (2011) 547-561.

[6] G. Drion, L. Massotte, R. Sepulchre, V. Seutin V, How modeling can reconcile apparently discrepant experimental results: the case of pacemaking in dopaminergic neurons. PLoS Comput. Biol. 7 (2011) e1002050.

[7] B. Hassard, Bifurcation of periodic solutions of the Hodgkin-Huxley model for the squid giant axon. J. Theor. Biol. 71 (1978) 401-420.

[8] E.N. Best, Null space in the Hodgkin-Huxley equations a critical test. Biophys J 27 (1979) 87-104.

[9] K. Aihara, G. Matsumoto, Two stable steady states in the Hodgkin-Huxley axons. Biophys J 41 (1983) 87-89.

[10] H. Fukai, S. Doi, T. Nomura, S. Sato, Hopf bifurcations in multiple-parameter space of the Hodgkin-Huxley equations I. Global organization of bistable periodic solutions. Biol. Cybern. 82 (2000) 215-222.

[11] J.Guckenheimer, R.A. Oliva, Chaos in the Hodgkin-Huxley model. SIAM J. App. Dyn. Sys. 1 (2002)105-114.

[12] D. Calitoiu, B.J. Oommen, D. Nussbaum, Spikes annihilation in the Hodgkin-Huxley neuron. Biol. Cybern. 98 (2008) 239-257.

[13] Y. Horikawa, Noise effects on spike propagation in the stochastic Hodgkin-Huxley models. Biol. Cybern. 66 (1991)19-25.

[14] D. Brown, J-F. Feng, S. Feerick, Variability of firing of Hodgkin- Huxley and FitzHugh-Nagumo neurons with stochastic synaptic input. Phys. Rev. Lett. 82 (1999) 4731-4734.

[15] P.H.E. Tiesinga, J.V. José, T.J. Sejnowski, Comparison of current-driven and conductance-driven neocortical model neurons with Hodgkin-Huxley voltage-gated channels. Phys. Rev. E 62 (2000) 8413-8419.

[16] T.D. Austin, The emergence of the deterministic Hodgkin-Huxley equations as a limit from the underlying stochastic ion-channel mechanism. Ann. Appl. Prob. 18 (2006) 1279-1325.

[17] M. Ozer, L.J. Graham LJ, Impact of network activity on noise delayed spiking for a Hodgkin-Huxley model. Eur. Phys. J. B 61 (2008) 499-503.

[18] R. Guttman, L. Feldman, H. Lecar, Squid axon membrane response to white noise stimulation. Biophys J 14 (1974) 941-955.

[19] H. Bryant, J.P. Segundo, Spike initiation by transmembrane current: a white-noise analysis. J. Physiol. 260 (1976), 279-314.

[20] R. Guttman, R. Grisell, L. Feldman, Strength-frequency relationship for white noise stimulation of squid axons. Math. Biosci. 33 (1977) 335-343

[21] D. Paydarfar, D.B. Forger, J.R. Clay, Noisy inputs and the induction of on-off switching behavior in a neuronal pacemaker. J. Neurophysiol. 96 (2006) 3338-3348.

[22] H.C. Tuckwell, J.Jost, B.S. Gutkin, Inhibition and modulation of rhythmic neuronal spiking by noise. Phys. Rev. E 80 (2009) 031907.

[23] H.C. Tuckwell, J. Jost, Moment analysis of the Hodgkin-Huxley system with additive noise. Physica A 388 (2009) 4115-4125.

[24] H.C.Tuckwell, J. Jost, Weak noise powerfully inhibits rhythmic spiking but not its propagation. PLoS Comp. Biol. 6 (2010) e1000794.

[25] H.C. Tuckwell, J. Jost, The effects of various spatial distributions of weak noise on rhythmic spiking. J. Comp. Neurosci. 30 (2011) 361-371.

[26] L. Gammaitoni, P. Hänggi, P. Jung, F. Marchesoni, Stochastic resonance. Rev. Mod. Phys. 70 (1998) 223-287.

[27] M. D. McDonnell, L. M. Ward, The benefits of noise in neural systems: bridging theory and experiment. Nat. Rev. Neurosci. 12 (2011) 415-426.

[28] D. Guo, Inhibition of rhythmic spiking by colored noise in neural systems. Cogn Neurodyn. 5 (2011) 293-300.

[29] R. Rodriguez, H.C. Tuckwell, Statistical properties of stochastic nonlinear dynamical models of single spiking neurons and neural networks. Phys. Rev. E 54 (1996) 5585-5590.

[30] P.E. Kloeden, E. Platen, A survey of numerical methods for stochastic differential equations. Stoch. Hydrol. Hydraul. 3 (1989) 155-178.

[31] H.C. Tuckwell. Introduction to Theoretical Neurobiology, Volume 2. Cambridge University Press, Cambridge UK, 1988.

[32] H.C. Tuckwell, Spike trains in a stochastic Hodgkin-Huxley system. BioSystems 80 (2005) 25-36.

[33] J. Jost, Dynamical Systems, Springer, Berlin, 2005.

[34] H. C. Tuckwell, Stochastic Processes in the Neurosciences, SIAM, Philadelphia, 1989.

[35] J. H. Goldwyn, N. S. Imennov, M. Famulare, E. Shea-Brown, Stochastic differential equation models for ion channel noise in Hodgkin-Huxley neurons. Phys. Rev. E 83 (2011) 041908.

[36] J. H. Goldwyn, E. Shea-Brown, The what and where of adding channel noise to the Hodgkin-Huxley equations. PLoS Comput Biol 7 (2011) e1002247.